INVESTIGATION OF AN OBLIQUE SHOCK WAVE-BOUNDARY LAYER INTERACTION

by

George U. Loffert, Jr.

A Thesis Submitted to the Faculty of the

AEROSPACE AND MECHANICAL ENGINEERING DEPARTMENT

In Partial Fulfillment of the Requirements
For the Degree of

MASTER OF SCIENCE

In the Graduate College

THE UNIVERSITY OF ARIZONA

1 9 6 4

STATEMENT BY AUTHOR

This thesis has been submitted in partial fulfillment of requirements for an advanced degree at The University of Arizona and is deposited in the University Library to be made available to borrowers under rules of the Library.

Brief quotations from this thesis are allowable without special permission, provided that accurate acknowledgment of source is made. Requests for permission for extended quotation from or reproduction of this manuscript in whole or in part may be granted by the head of the major department or the Dean of the Graduate College when in his judgment the proposed use of the material is in the interests of scholarship. In all other instances, however, permission must be obtained from the author.

SIGNED: George H. Tolbert Jr.

APPROVAL BY THESIS DIRECTOR

This thesis has been approved on the date shown below:

E. K. Parks — APRIL 28/64

E. K. PARKS — Date

Professor of Aerospace and Mechanical Engineering

ACKNOWLEDGMENTS

The author wishes to express his indebtedness to Dr. E. K. Parks for his assistance, encouragement, and patience, without which this study would have been impossible.

To Mr. 橋爪 宏 (Hiroshi Hashizume), of the National Aerospace Laboratory, Tokyo, Japan, for his experienced advice; to graduating seniors Salvator Balsamo, Richard Brusch, and Ronald Phelan for their assistance in the laboratory; and to Mr. Gerard Fields who constructed the test model, the author is indeed grateful.

For her patience and understanding throughout my graduate schooling, I thank my wife, Gloria, and to Miss Irene Schick who typed the manuscript, I express my sincere appreciation for her diligence and professional work.

TABLE OF CONTENTS

LIST OF ILLUSTRATIONS

LIST OF ILLUSTRATIONS
(Continued)

LIST OF TABLES

LIST OF SYMBOLS

x = distance from leading edge of the flat plate parallel to the surface

y = distance from the flat plate measured normal to the surface

u = component of velocity in boundary layer parallel to surface

U = free stream velocity

p = pressure

ρ = density

μ = dynamic viscosity

γ = ratio of specific heat at constant pressure to specific heat at constant volume. For air, $\gamma = 1.4$

M = free stream Mach number

Re_x = Reynolds number with respect to leading edge of plate

δ = boundary layer thickness

δ^* = boundary layer displacement thickness

θ = deflection angle of free stream from the plate

n, λ = parameters in assumed velocity profile for laminar boundary layer

The suffix 1 indicates boundary layer conditions for zero pressure gradient.

ABSTRACT

Knowledge of the effects of shock wave interaction with laminar and turbulent boundary layers, particularly the conditions for separation of the boundary layer, is an important area of interest in the design of supersonic aircraft and other aerospace vehicles. This thesis is primarily concerned with the propagation of pressures within the boundary layer due to the interaction of an oblique, externally generated shock wave. Theoretical expressions are developed for the prediction of separation for both laminar and turbulent boundary layers. The validity of these predictions was then checked experimentally in the University of Arizona supersonic wind tunnel at a Mach number of 3.2.

Experimental results showed that the theoretical predictions for pressure ratio at separation of the laminar boundary layer were reasonably close to the experimental values, being a function of Mach number and Reynolds number only and independent of shock strength. For the turbulent interactions this pressure ratio, dependent upon Mach number only, was found to be higher than the experimental values. Turbulent boundary layers proved to be highly resistant to external disturbances, requiring much greater shock strengths than a laminar boundary layer to cause the same separation conditions. The general interaction phenomena observed experimentally agreed quite well with the theoretical analysis.

CHAPTER 1

INTRODUCTION

1.1 General Considerations

Many aerospace problems in fluid dynamics, such as flow through jet intake ducts and flow past wings or control surfaces, involve the interaction of shock waves with the boundary layer of the surface under consideration. According to Prandtl's flow model, viscous effects of fluid flow past a surface can be neglected except in a very thin region close to the surface known as the boundary layer. These viscous effects in turn can be investigated separately by boundary layer theory. The flow external to the boundary layer is generally independent of the boundary layer flow in the absence of separation or other large pressure gradients. However, the boundary layer flow is greatly affected by longitudinal pressure changes in the external flow field. Since the pressure change across a shock wave is considerable, it is reasonable to assume that the interaction of a shock wave with a boundary layer will cause the flow in the boundary layer to become distorted, which in turn can affect the external flow field. It is this interaction, in this case an externally generated shock wave impinging on either a laminar or a turbulent boundary layer on a flat plate, which will be considered in this investigation.

1.2 A Physical Description of the Interaction Phenomena

In the absence of viscous effects, the reflection of an oblique shock wave from a flat surface is a rather simple problem which can be solved quickly with the help of shock tables. The static pressure distribution on the surface of the plate can be calculated for a particular Mach number and incident angle as shown in Figure 1.01(a).

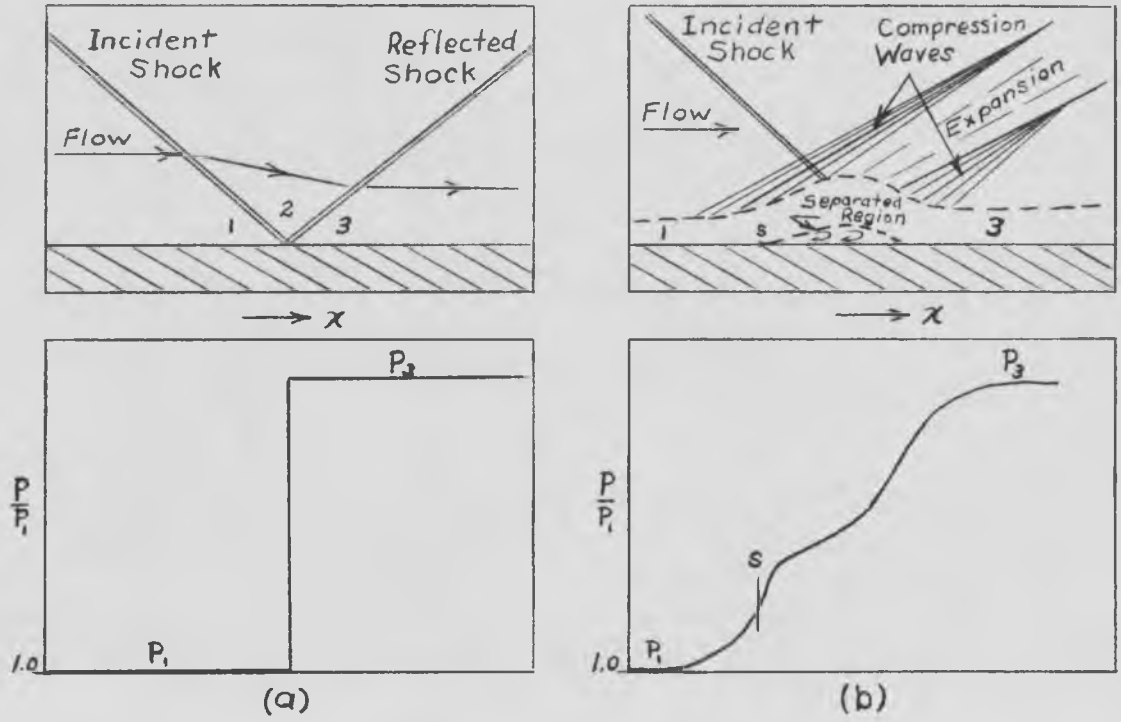

Figure 1.01 Reflection conditions and pressure distributions for same Mach number and longitudinal scale for (a) regular reflection (no boundary layer), (b) boundary layer interaction.

A boundary layer in supersonic flow has an appreciable portion of its thickness which is subsonic. The pressure discontinuity caused by the impingement of a shock wave can be transmitted both upstream and downstream from the point of impingement in this subsonic portion of the

boundary layer. Propagation of pressures upstream causes thickening of the boundary layer and may lead to separation of the boundary layer for certain shock wave and boundary layer conditions as shown in Figure 1.01(b). Static pressure distribution is seen to be quite different from the regular reflection if Figure 1.01(a). The propagation of pressures in both laminar and turbulent boundary layers, and related separation phenomena, will be investigated in this study.

1.3 Method of Investigation

A boundary layer was established on a flat plate in the test section of the supersonic wind tunnel of the Department of Aerospace and Mechanical Engineering, University of Arizona. Above the flat plate a shock wave generator with a variable deflection angle produced shock waves of variable strength which impinged on the flat plate. Static pressure readings were taken by means of pressure taps near the centerline of the plate and recorded on a Leeds and Northrup recording potentiometer through a Statham pressure transducer. The Reynolds number of the point of impingement was varied by moving the shock generator longitudinally. For the turbulent studies a boundary layer trip wire was affixed to the front of the plate.

For a particular configuration of the test model, a schlieren photograph was taken in each case to record the flow pattern as the static pressure readings were being taken. These photographs are discussed along with the experimental results of this study in Chapter 3. In Chapter 2 the theoretical considerations of the flow will be

investigated using experimental results of previous studies in addition to boundary layer theory.

CHAPTER 2

THEORETICAL CONSIDERATIONS

2.1 Separation Phenomena

This investigation will deal with the two-dimensional interaction of an oblique shock wave with both laminar and turbulent boundary layers. In most cases considered the shock wave is strong enough to cause separation of the boundary layer. It will be assumed that at the point of impingement of the shock wave the boundary layer is either laminar or turbulent, not in the region of transition. Since the physical phenomena of both laminar and turbulent boundary layers is similar, this section will deal with both cases. In Sections 2.2 and 2.3 the pressure relationships for separation in laminar and turbulent cases respectively will be investigated.

In the case of a shock wave strong enough to separate the boundary layer, the pressure propagation toward the leading edge causes the boundary layer to thicken and separate upstream of the point of interaction. Figure 2.01 shows the general case of shock wave-boundary layer interaction with separation.

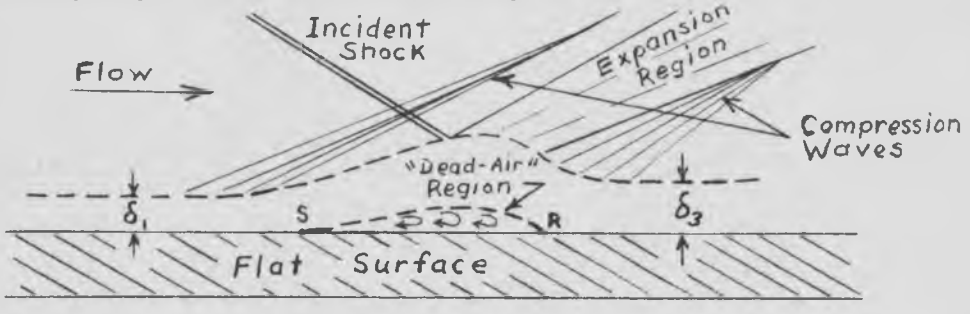

Figure 2.01 Shock Wave-Boundary Layer Interaction With Separation.

According to a study by G. E. Gadd (Ref. 1) the pressure ratio at separation should be a function of Mach number and Reynolds number only, being independent of shock strength. He reasons that the thickening of the boundary layer ahead of the point of incidence induces a band of compression waves, as shown in Figure 2.01, which determine the pressure distribution on the boundary layer upstream of the interaction point. This pressure distribution in turn affects the rate of thickening of the boundary layer. Since the two processes reach equilibrium, the pressure distribution upstream of the initial point of impingement should remain the same if the shock strength is increased and the interaction point moved downstream to a position where the separation point remains in its initial position. Using this reasoning he concludes that the separation pressure ratio is independent of shock strength and dependent upon Mach number and Reynolds number only. Studies by Barry, Shapiro, and Neumann (Ref.2), and Kepler and Bogdonoff (Ref. 3) tend to bear out Gadd's reasoning.

Moving downstream from the interaction point along the outer edge of the boundary layer in Figure 2.01, we note that the impinging shock wave is reflected initially as an expansion wave. Without the expansion there would be a discontinuous jump in pressure, as in the case of a regular reflection, which the separated boundary layer could not withstand. Note that the flow is turned toward the plate by the expansion wave and then as the flow is turned back parallel to the plate a compression wave system will cause the pressure to rise higher.

Downstream of the separation point there is a "pocket" or "dead air" region next to the plate. Immediately to the rear of the separation point where this area is relatively thin it can still sustain a fairly large adverse pressure gradient due mainly to viscous friction forces. As the dead air region grows thicker it can no longer sustain a large adverse pressure gradient since the viscous friction forces are decreased as the rate of change of friction stress normal to the plate becomes small. In order to maintain equilibrium conditions the pressure gradient should decrease in this thick separated area where the boundary layer is deflected away from the plate. At the point of interaction of the shock wave and the boundary layer the flow is turned back toward the plate and the thickness of the separated area is decreased until the reattachment point is reached. In this region a larger adverse pressure gradient can be supported by the boundary layer and the pressure should increase up to a point behind the reattachment of the boundary layer. Experimental studies show that this analysis is generally true for both laminar and turbulent boundary layers. However, turbulent boundary layers require much stronger shocks to create the same effects as for laminar boundary layers. The turbulent layers are able to withstand adverse pressure gradients better than laminar boundary layers due in part to the greater momentum of the layer as a result of turbulence. Also, for turbulent boundary layers, Gadd (Ref. 1) proposes that mass acceleration effects play a significant part in the equilibrium of the separated region.

An explanation for the movement of the separation point upstream upon increasing the shock strength can follow an argument similar to the one above concerning the shape of the interaction area. At the point of shock wave interaction the pressure is not influenced very much by the distance of the separation point upstream due to the relatively small pressure gradient in the region between separation and the point of interaction. If the shock strength is increased the flow will be turned toward the plate more sharply in the expansion region just behind the interaction point. Since the boundary layer will not be able to support any further increase in adverse pressure gradient and remain in equilibrium, the curvature of the boundary layer between the point of interaction and the point of reattachment cannot increase. Now the thickness of the boundary layer at the point of reattachment will increase due to the increased pressure from the stronger shock. Therefore, for the external flow to conform to the shape of the boundary layer, the thickness of the boundary layer must be greater at the point of impingement as shown in Figure 2.02.

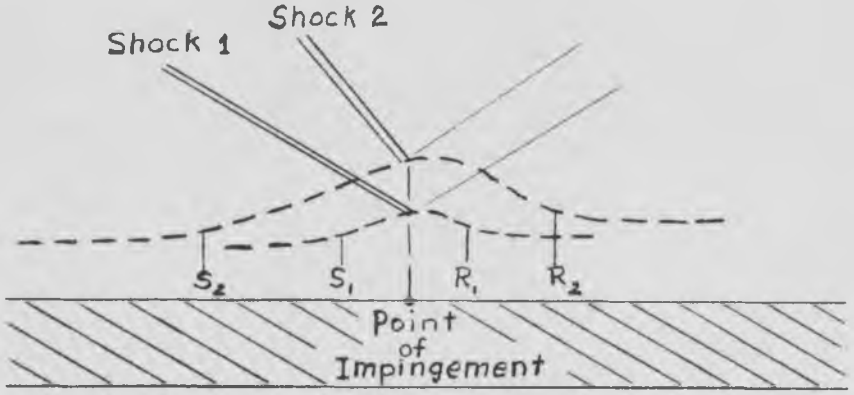

Figure 2.02 Interaction area for shocks 1 and 2 where shock 2 is greater than shock 1. S and R are separation and reattachment points respectively.

This forces the separation point to move farther upstream of the shock wave interaction point.

The separation phenomena discussed above applies generally to both laminar and turbulent boundary layers as mentioned previously. Although the physical effects on the boundary layer are similar, the analysis leading up to an expression for the pressure ratio at separation is of necessity quite different due to the great difference in velocity profiles of laminar and turbulent boundary layers. Sections 2.2 and 2.3 deal with laminar and turbulent separation respectively.

2.2 Laminar Interaction - Pressure Ratio for Separation

In this section an approximate method for predicting the pressure ratio at separation will be developed following the methods used by G. E. Gadd (Ref. 1) and A. D. Young (Ref. 4). It is considered more accurate than the Pohlhausen method for incompressible flow in cases where small pressure increases and large pressure gradients occur after a relatively long region of zero pressure gradient.

The velocity profile for the region where the pressure gradient is zero upstream of the shock interaction point (we shall designate it station 1) will be assumed to be of the form

$$\frac{u}{U_1} = \sin\left[\frac{\pi}{2}\left(\frac{y}{\delta_1}\right)\right] \tag{1}$$

after Gadd's analysis. Assuming the Prandtl number is unity, that there is no heat transfer to the plate and that $\frac{\mu}{\mu_1} = \frac{T}{T_1}$,

$$\mu = \left[1 + (1 - u^2/U_1^2)\,\frac{\gamma-1}{2}\,M_1^2\right]\mu_1$$

$$\rho = \frac{p}{p_1\left[1 + (1 - u^2/U_1^2)\frac{\gamma-1}{2} M_1^2\right]} \rho_1$$

Using these relationships with Equation (1) and defining the displacement thickness as $\delta^* = \int_0^\delta \left(1 - \frac{\rho u}{\rho_1 U_1}\right) dy$ the displacement thickness for zero pressure gradient becomes,

$$\delta_1^* = \delta_1 \left\{1 - \frac{2 \tan^{-1}\left[\left(\frac{\gamma-1}{2}\right)^{1/2} M_1\right]}{\pi \left[\left(\frac{\gamma-1}{2}\right)^{1/2} M_1\right]}\right\}$$

According to A. D. Young (Ref. 4) a good empirical equation for this displacement thickness is,

$$\delta^* = 1.721\left[1 + 0.693(\gamma-1)M_1^2\right] \frac{x}{\sqrt{Re_x}} \qquad (2)$$

where $R_{ex} = \frac{\rho_1 U_1 x}{\mu_1}$. Therefore, equating and solving for δ_1,

$$\delta_1 = \frac{1.721\left[1 + 0.693(\gamma-1)M_1^2\right] x}{\left\{1 - \frac{2 \tan^{-1}\left[\left(\frac{\gamma-1}{2}\right)^{1/2} M_1\right]}{\pi \left[\left(\frac{\gamma-1}{2}\right)^{1/2} M_1\right]}\right\} \sqrt{Re_x}} \qquad (3)$$

As the pressure begins to increase the velocity profile downstream changes as shown in Figure 2.03(a).

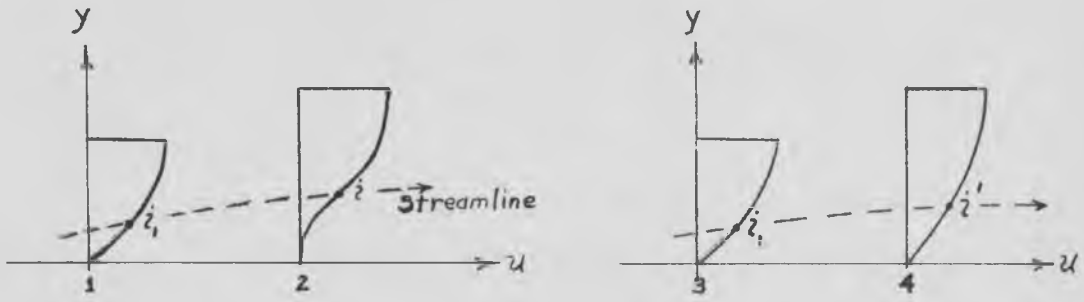

(a) Adverse pressure gradient between points 1 and 2

(b) No pressure gradient between 3 and 4

Figure 2.03 Velocity profiles in laminar boundary layer for (a) adverse pressure gradient, (b) no pressure gradient.

The points $\dot{\imath}$ and $\dot{\imath}_1$, and $\dot{\imath}'$ and $\dot{\imath}_1$ on the profiles are on the same streamline, point $\dot{\imath}$ being the approximate inflection point with an adverse pressure gradient. If the pressure gradient between points 1 and 2 is very great, the forces acting on the fluid above the point $\dot{\imath}$ would be governed mainly by the pressure gradient forces and the viscous forces could be neglected. Therefore, the outer profile at station 2 could be derived from that at station 1 using the continuity equation and Bernoulli's equation. If the pressure gradient is not great however, the viscous forces cannot be ignored. Figure 2.03(b) shows the velocity profiles for no pressure change. Again, points $\dot{\imath}'$ and $\dot{\imath}_1$ are on the same streamline. The upper part of the profile in Figure 2.03(a) above point $\dot{\imath}$ is nearly the same as that above point $\dot{\imath}'$ in Figure 2.03(b). The profile will be broken down for analysis into the upper and lower portions. The upper portion will be treated according to inviscid fluid theory and the lower portion by other methods.

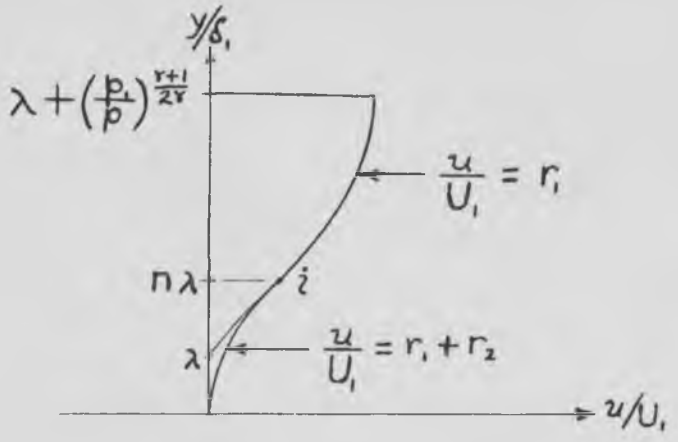

Figure 2.04 Assumed velocity profile for a laminar boundary layer with adverse pressure gradient.

Figure 2.04 shows the assumed profile with an adverse pressure gradient, where λ is an arbitrary constant dependent upon the distance of the inflection point i from the plate. Since the outer profile is to be treated according to inviscid fluid theory and remains sinusoidal according to Equation (1), the modified outer profile becomes

$$\frac{u}{U_1} = \sin\left[\pi/2\left(\frac{p}{p_1}\right)^{\frac{\gamma+1}{2\gamma}}\left(y/\delta_1 - \lambda\right)\right] = r_1$$

It can be seen that for zero pressure gradient this profile remains as in Equation (1) thus,

$$\frac{u}{U_1} = \sin\left[\pi/2\left(\frac{p_1}{p_1}\right)^{\frac{\gamma+1}{2\gamma}}\left(y/\delta_1 - \lambda^{0}\right)\right] = \sin\left[\pi/2\left(y/\delta_1\right)\right]$$

Also, the y/δ_1 coordinate at the outer edge of the boundary layer, where $\frac{u}{U_1} = r_1 = 1$ is, $\left(\frac{p}{p_1}\right)^{\frac{\gamma+1}{2\gamma}}\left(y/\delta_1 - \lambda\right) = 1$

$$\left(y/\delta_1 - \lambda\right) = \frac{1}{\left(\frac{p}{p_1}\right)^{\frac{\gamma+1}{2\gamma}}} = \left(\frac{p_1}{p}\right)^{\frac{\gamma+1}{2\gamma}}$$

$$\therefore\ y/\delta_1 = \lambda + \left(\frac{p_1}{p}\right)^{\frac{\gamma+1}{2\gamma}}$$

as shown in Figure 2.04.

For the part of the profile below the inflection point $\dot{i}$ the expression for the term to be added to the velocity profile, r_2, must meet the conditions that it is zero at $\frac{y}{\delta_1} = n\lambda$ and exactly equal and opposite in sign to the value of r_1 at $\frac{y}{\delta} = 0$. Therefore, after Gadd's analysis, $r_2 = (1 - y/n\lambda\delta_1)^3 \sin\left[\pi/2 \left(\frac{p}{p_1}\right)^{\frac{r+1}{2r}} \lambda\right]$ and the lower part of the velocity profile becomes,

$$\frac{u}{U_1} = r_1 + r_2 = \sin\left[\pi/2 \left(\frac{p}{p_1}\right)^{\frac{r+1}{2r}} \left(y/\delta_1 - \lambda\right)\right] + (1 - y/n\lambda\delta_1)^3 \sin\left[\pi/2 \left(\frac{p}{p_1}\right)^{\frac{r+1}{2r}} \lambda\right]$$

Figure 2.05 shows the construction of the lower profile graphically.

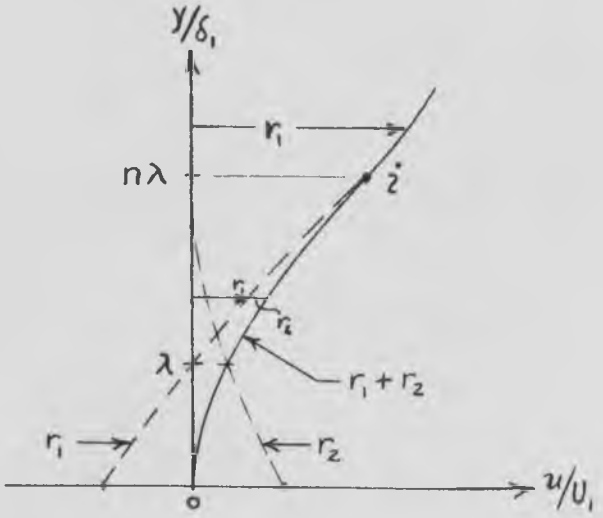

Figure 2.05 Graphical representation of the addition of curves to obtain the lower velocity profile with adverse pressure gradient.

Therefore the velocity profile with an adverse pressure gradient becomes,

$$\frac{u}{U_1} = r_1 \quad \text{for} \quad n\lambda < y/\delta_1 < \lambda + \left(\frac{p}{p_1}\right)^{\frac{r+1}{2r}}$$

$$\frac{u}{U_1} = r_1 + r_2 \quad \text{for} \quad 0 < y/\delta_1 < n\lambda \qquad (4)$$

Since $\dot{\imath}_1$ and $\dot{\imath}$ are on the same streamline between stations 1 and 2, the mass flow between these points and the plate must be the same, as must the flow between $\dot{\imath}_1$ and $\dot{\imath}'$ and the plate in Figure 2.03(b). This continuity condition is met approximately by the equation

$$\frac{\pi^2}{16}\lambda^2(n-2) = \frac{(1+\frac{\gamma-1}{2}M_1^2)(p-p_1)}{\gamma M_1^2 p_1} \tag{5}$$

if $\frac{p-p_1}{p_1}$ and λ are small, for example $1 < \frac{p}{p_1} < 1.2$ and $\cos(\pi/2\,\lambda) \approx 1-(\pi^2\lambda^2/4)$.

Near the plate the viscous forces must balance the pressure gradient, so $dp/dx = \mu \frac{\partial^2 u}{\partial y^2}$

Therefore, $$\frac{dp}{dx} = \frac{3\pi\mu_1 U_1}{n^2 \lambda \delta_1^2}\left(1+\frac{\gamma-1}{2}M_1^2\right) \tag{6}$$

Now Equations (4), (5), (6) relate the velocity profile to the pressure and pressure gradient. Since the pressure is related to the displacement thickness δ^*, Equations (2), (3), and (4) can be used to arrive at an approximate equation for the displacement thickness, assuming $(n-2)\lambda < 0.25$,

$$\delta^* = \delta_1^* + \lambda\delta_1 \tag{7}$$

Assuming pressure changes to be small, the deflection angle Θ of the free stream from the plate upstream of the shock

interaction point is related to pressure by the relationship

$$\theta = \frac{\sqrt{M_1^2 - 1}}{\gamma M_1^2} \left(\frac{p - p_1}{p_1} \right)$$

This may be derived using small perturbation theory according to Liepmann and Roshko (Ref. 5) as follows:

$$C_p = \frac{2}{\gamma M_\infty^2} \left(\frac{p - p_\infty}{p_\infty} \right)$$

but from thin airfoil theory, $C_p = \frac{2\theta}{\sqrt{M^2 - 1}}$ for two-dimensional supersonic flow. Therefore, using station 1 as a reference,

$$\frac{2\theta}{\sqrt{M_1^2 - 1}} = \frac{2}{\gamma M_1^2} \left(\frac{p - p_1}{p_1} \right)$$

$$\therefore \theta = \frac{\sqrt{M_1^2 - 1}}{\gamma M_1^2} \left(\frac{p - p_1}{p_1} \right)$$

With a flat plate, θ is also assumed to be

$$\theta = \frac{d\delta^*}{dx} - \frac{d\delta_1^*}{dx}$$

where θ is small. Therefore, in this region

$$\frac{d}{dx} \left(\delta^* - \delta_1^* \right) = \frac{\sqrt{M_1^2 - 1}}{\gamma M_1^2} \left(\frac{p - p_1}{p_1} \right) \tag{8}$$

According to Gadd (Ref. 1), the above analysis assuming an outer inviscid flow and an inner viscous flow corresponds quite closely to an exact mathematical analysis for small perturbations.

At the separation point, Equation (8) becomes

$$\frac{d}{dx}\left(\delta^* - \delta_1^*\right) = \frac{\sqrt{M_1^2 - 1}}{\gamma M_1^2}\left(\frac{p_s - p_1}{p_1}\right)$$

and $\frac{d}{dx}\left(\delta^* - \delta_1^*\right) = 0$ at station 1. If $\left(\delta^* - \delta_1^*\right)$ is assumed to vary parabolically with x in the interval from station 1 to the separation point,

$$x_s - x_1 \approx \frac{\left(\delta^* - \delta_1^*\right)_s - \left(\delta^* - \delta_1^*\right)_1}{1/2\left[\frac{d}{dx}\left(\delta^* - \delta_1^*\right)\right]_s}$$

$$x_s - x_1 = \frac{(\delta_1\lambda)_s - \cancel{(\delta_1\lambda)_1}^{\,0}}{\frac{1}{2}\left[\frac{\sqrt{M_1^2 - 1}}{\gamma M_1^2}\left(\frac{p_s - p_1}{p_1}\right)\right]} \qquad \text{using (7) \& (8)}$$

$$\therefore\ x_s - x_1 = 2\left(\delta_1\lambda\right)_s \left(\frac{\gamma M_1^2}{\sqrt{M_1^2 - 1}}\right)\left(\frac{p_1}{p_s - p_1}\right)$$

Also, by Equation (6) with $n = 3$ at the separation point,

$$p_s - p_1 \approx \frac{1}{2}\left(\frac{dp}{dx}\right)_s \left(x_s - x_1\right)$$

$$= \frac{\pi \mu_1 U_1 \left(1 + \frac{\gamma - 1}{2} M_1^2\right)\gamma M_1^2}{3\,\delta_{1_s}\sqrt{M_1^2 - 1}}\left(\frac{p_1}{p_s - p_1}\right)$$

Therefore, at separation the pressure ratio using Equation (3) and

$$\frac{x_s}{\sqrt{Re_{x_s}}} = \frac{\mu_1}{\rho_1 U_1} = \frac{\mu_1 U_1}{\rho_1 U_1^2} = \frac{\mu_1 U_1}{\frac{\gamma p_1 U_1^2}{\gamma R T_1}} = \frac{\mu_1 U_1}{\gamma p_1 M_1^2} \quad ,$$

$$\frac{(p_s - p_1)^2}{p_1} = \frac{\pi \mu_1 U_1 \left(1 + \frac{\gamma - 1}{2} M_1^2\right)\gamma M_1^2}{3\,\delta_{1_s}\sqrt{M_1^2 - 1}}$$

$$\frac{(p_s - p_1)^2}{p_1} = \frac{\pi \mu_1 U_1 \left(1 + \frac{\gamma-1}{2} M_1^2\right) \gamma M_1^2}{3\sqrt{M_1^2 - 1}} \left\{ \frac{1.721 \left[1 + 0.693(\gamma-1) M_1^2\right] x_s}{1 - \left[\frac{0.636 \tan^{-1}\left[\left(\frac{\gamma-1}{2}\right)^{1/2} M_1\right]}{\left(\frac{\gamma-1}{2}\right)^{1/2} M_1}\right] \sqrt{Re_{x_s}}} \right\}$$

$$= \frac{\pi \mu_1 U_1 \left(1 + \frac{\gamma-1}{2} M_1^2\right) \gamma M_1^2 \left[1 - \frac{0.636 \tan^{-1}\left[\left(\frac{\gamma-1}{2}\right)^{1/2} M_1\right]}{\left(\frac{\gamma-1}{2}\right)^{1/2} M_1}\right]}{3\sqrt{M_1^2 - 1} \left(1.721 \left[1 + 0.693(\gamma-1) M_1^2\right]\right) \left(\frac{x_s}{\sqrt{Re_{x_s}}}\right) \frac{\sqrt{Re_{x_s}}}{\sqrt{Re_{x_s}}}}$$

$$= \frac{\pi \mu_1 U_1 \left(1 + \frac{\gamma-1}{2} M_1^2\right) \gamma M_1^2 \left[1 - \frac{0.636 \tan^{-1}\left[\left(\frac{\gamma-1}{2}\right)^{1/2} M_1\right]}{\left(\frac{\gamma-1}{2}\right)^{1/2} M_1}\right]}{3\sqrt{M_1^2 - 1} \left(1.721 \left[1 + 0.693(\gamma-1) M_1^2\right]\right) \frac{x_s \sqrt{Re_{x_s}}}{Re_{x_s}}}$$

Substituting for x_s / Re_{x_s}:

$$\frac{(p_s - p_1)^2}{p_1} = \frac{\pi \cancel{\mu_1 U_1} \left(1 + \frac{\gamma-1}{2} M_1^2\right) \gamma M_1^2 \left[1 - \frac{0.636 \tan^{-1}\left[\left(\frac{\gamma-1}{2}\right)^{1/2} M_1\right]}{\left(\frac{\gamma-1}{2}\right)^{1/2} M_1}\right]}{3\sqrt{M_1^2 - 1} \sqrt{Re_{x_s}} \left(1.721 \left[1 + 0.693(\gamma-1) M_1^2\right]\right) \left(\frac{\cancel{\mu_1 U_1}}{\gamma p_1 M_1^2}\right)}$$

$$\left(\frac{p_s - p_1}{p_1}\right)^2 = \left(\frac{\pi}{5.163}\right) \frac{(\gamma M_1^2)^2 \left(1 + \frac{\gamma-1}{2} M_1^2\right) \left[1 - \frac{0.636 \tan^{-1}\left[\left(\frac{\gamma-1}{2}\right)^{1/2} M_1\right]}{\left(\frac{\gamma-1}{2}\right)^{1/2} M_1}\right]}{\left[(M_1^2 - 1) Re_{x_s}\right]^{1/2} \left[1 + 0.693(\gamma-1) M_1^2\right]}$$

Finally, for Equation (9):

$$\frac{p_s - p_1}{p_1} = \frac{0.78 \gamma M_1^2}{\left[(M_1^2 - 1) Re_{x_s}\right]^{1/4}} \left\{ \frac{\left(1 + \frac{\gamma-1}{2} M_1^2\right) \left[1 - \frac{0.636 \tan^{-1}\left[\left(\frac{\gamma-1}{2}\right)^{1/2} M_1\right]}{\left(\frac{\gamma-1}{2}\right)^{1/2} M_1}\right]}{1 + 0.693(\gamma-1) M_1^2} \right\}^{1/2} \quad (9)$$

The above equation is valid up to Mach 4.0 according to experimental studies by Gadd (Ref. 1). The values applicable to this study will be computed and analyzed in Chapter 3.

2.3 Turbulent Interaction-Pressure Ratio for Separation

The approximate solution for pressure ratio at separation in turbulent flow developed in this section has no firm basis in theory. Its validity for Mach numbers up to 4.0 as investigated by Gadd (Ref. 1) is the main justification for its use. A more firm analysis similar to Section 2.2 for laminar flow would be preferable if there were better relationships available between the shape of the velocity profile in turbulent flow and turbulent friction stresses. However, for this study the method should be acceptable since all data in Chapter 3 was taken at Mach = 3.2.

A good approximation for the velocity profile in turbulent flow with zero pressure gradient was found by Monaghan and Johnson (Ref. 6) to be close to that for incompressible flow. Their experimental data was taken at M = 2.5 and found to be a good fit to the profile $\frac{u}{U_1} = \left(y/\delta_1\right)^{1/7}$ sketched in Figure 2.06. Since Gadd (Ref. 1) found it to be valid in the vicinity of M = 3.0, it will be assumed to fit the data in this study taken at M = 3.2.

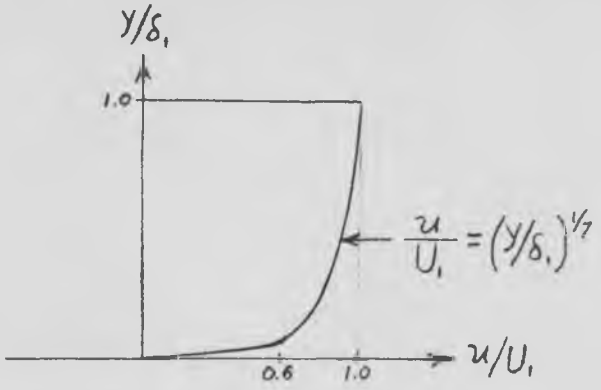

Figure 2.06 Assumed velocity profile in turbulent flow with zero pressure gradient.

Previous studies show that the pressure rises steeply to the separation point in turbulent boundary layers. It will be assumed that this large pressure gradient is great enough to make the friction forces relatively small except near the plate. Therefore, the changes in velocity in the outer portion of the boundary layer may be approximated by Bernoulli's equation, assuming temperature constant. Let Δp be the pressure increase necessary to bring the fluid at $\frac{u}{U_1} = 0.6$ to rest isentropically. At station 1 there is little fluid flow between $\frac{u}{U_1} = 0.6$ and the plate. If the pressure change is less than Δp there probably would be only a very thin separated region next to the plate, but for a pressure change greater than Δp all the higher velocity fluid at the shoulder of the velocity profile would be brought to rest, resulting in a thick separated region. Therefore, it is reasonable to believe that Δp is a fair approximation for the pressure rise at separation. An expression for the pressure ratio at separation, developed by Gadd (Ref. 1), using the above reasoning, is given below.

$$\frac{p_s}{p_1} = \left[\frac{1 + \frac{\gamma-1}{2} M_1^2}{1 + 0.64 \frac{\gamma-1}{2} M_1^2} \right]^{\frac{\gamma}{\gamma-1}} \qquad (10)$$

This equation will be used to predict the pressure ratio for separation of the turbulent boundary layer and is compared with the approximate separation points as observed on schlieren photographs in the following chapter dealing with experimental results. It is seen to be a function of the free stream Mach number only as compared to the laminar case where this pressure ratio is a function of both the free stream Mach number and the Reynolds number of the point of separation.

CHAPTER 3

EXPERIMENTAL RESULTS

3.1 Test Apparatus

A test model was designed and constructed as shown in Figure 3.01 for use in the 3" x 5" supersonic wind tunnel. It consisted of a flat steel plate with nine pressure taps staggered at 1/2 inch intervals along its centerline beginning two inches from the leading edge. These were connected to plastic tubing which led through the steel tubing mount to the outside of the test section. The plate had a sharp leading edge perpendicular to the flow direction with a 15 degree half-wedge lower nose section. This nose section was detachable to provide for lengthening the plate in order to change the Reynolds number. The surface of the plate was ground flat and then polished by hand to get as smooth a surface as possible.

Above the plate was mounted a shock generator arrangement composed of a small variable-incidence plate connected by a long sting to the rear of the main plate mount. This generator could be moved longitudinally to vary the shock wave interaction point on the boundary layer. It could also be adjusted vertically to any desired position.

The pressure taps were connected to a Statham 0-15 psid pressure transducer which was in turn connected to a Leeds and Northrup recording potentiometer. Figure 3.02 shows views of the test set up as it was used to record data.

To record the shock wave-boundary layer interaction pictorially a schlieren system was used to photograph each run when a particular parameter was changed. A ground-glass viewing screen in place of the film pack permitted each data run to be monitored if a picture was not being taken. Figure 3.03 is a diagram of the schlieren system used.

Photographs of the University of Arizona 3" x 5" wind tunnel are shown in Figures 3.02 and 3.04. It is a suck-down type with a 1200 cubic foot vacuum tank capacity. A Stokes 300 cfm vacuum pump is connected to the vacuum tank by way of the valving arrangement shown. The area ratio can be varied by adjusting the moveable nozzle blocks to produce test section Mach numbers from $M = 1.5$ to $M = 5.2$. An adjustable diffuser section provides optimum diffuser settings for any given area ratio between the first throat and the test section.

3.2 Test Procedure

During the period of data-taking, the test apparatus for this study had to be removed from the test section between data sessions due to use of the tunnel for other projects. Therefore, a standard procedure had to be followed to insure that conditions for each run were as much alike as possible. Before each series of runs with shock wave interaction, a pressure traverse was made without the shock generator attached to obtain a reference pressure for each pressure tap under the existing atmospheric conditions. The Mach number was obtained by pressure measurement and checked by angle measurement from

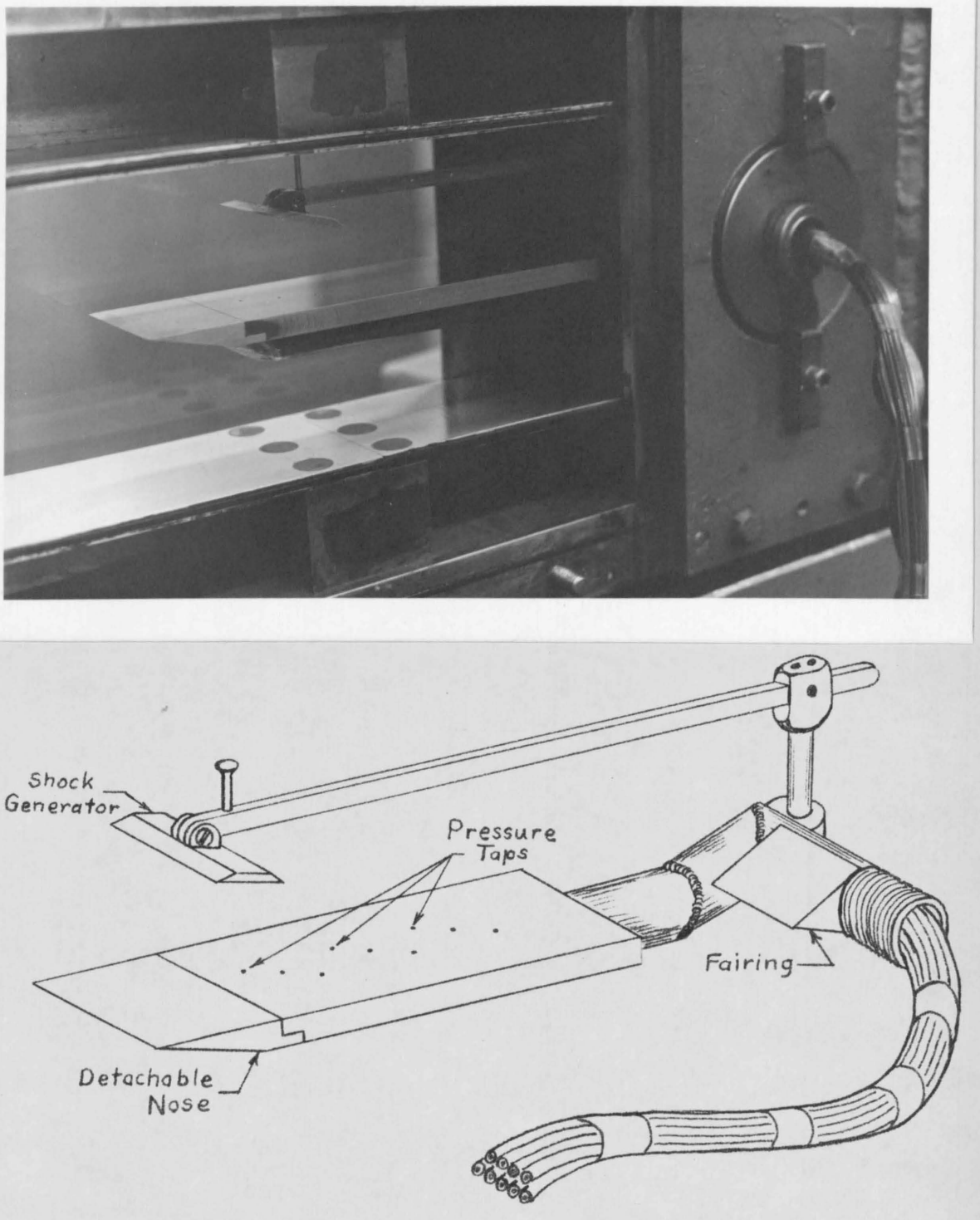

Figure 3.01 Test model for shock wave-boundary layer interaction on a flat plate.

Figure 3.02 Test arrangement for wind tunnel experimentation.

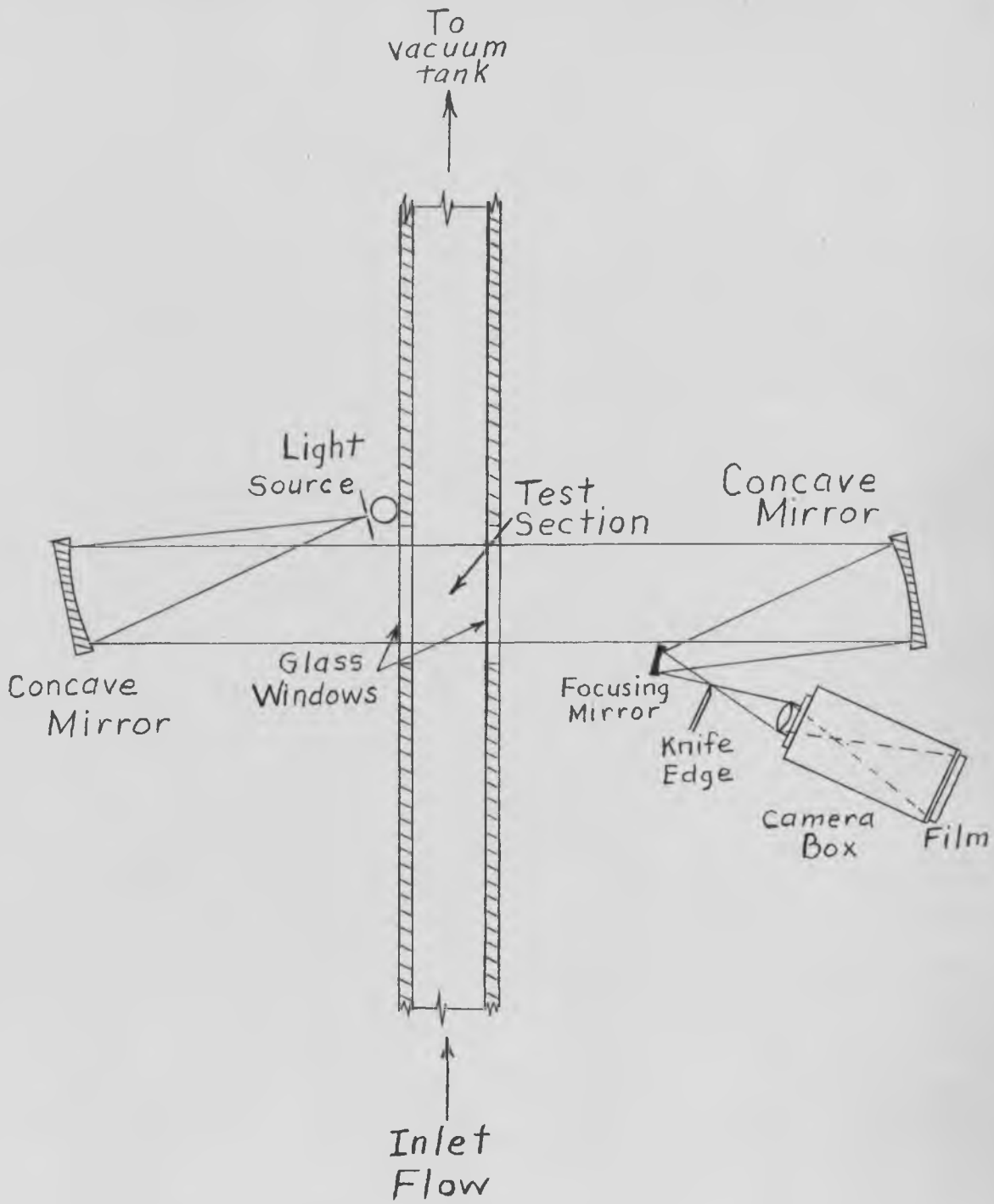

Figure 3.03 Diagram of schlieren system with concave mirrors.

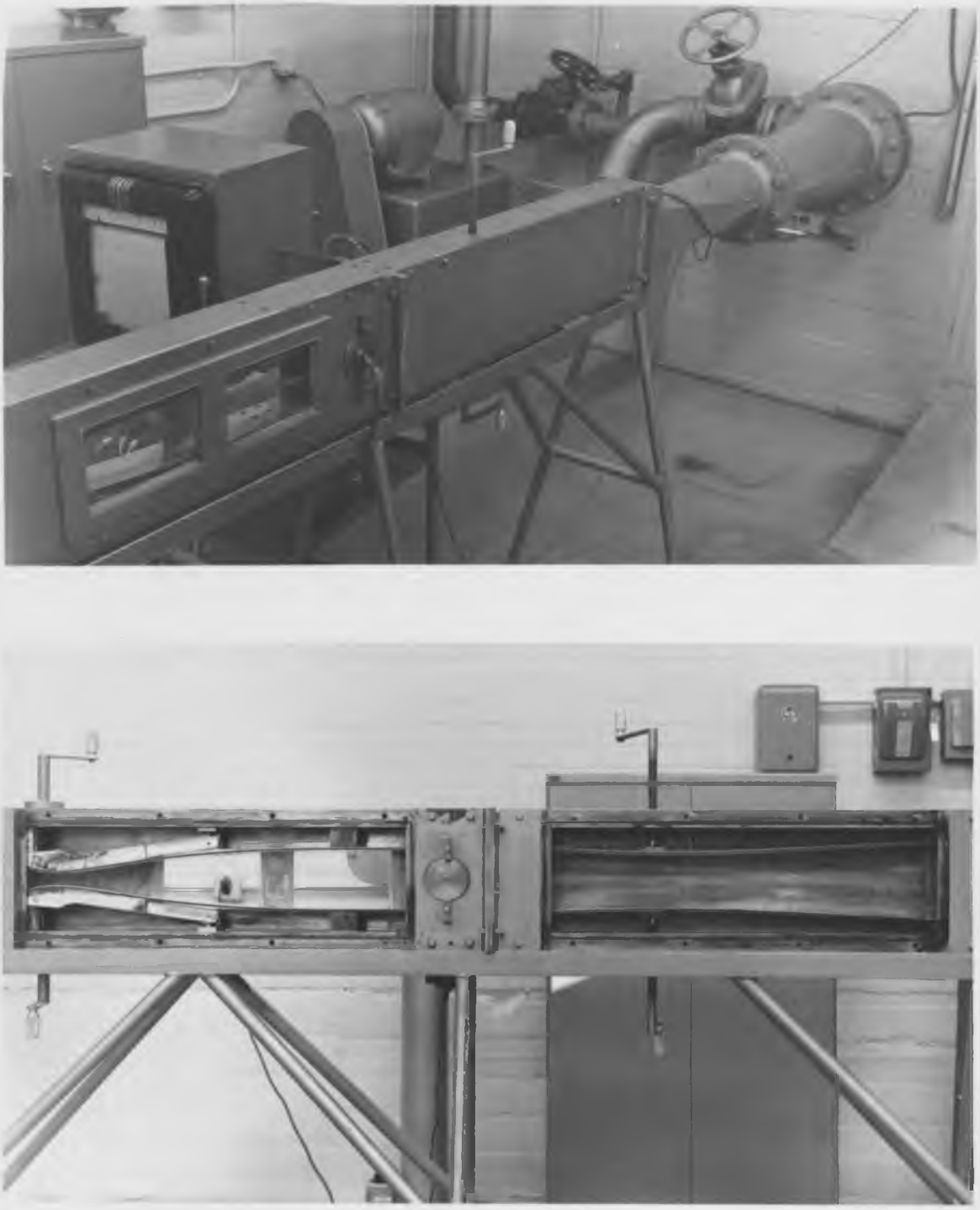

Figure 3.04 Details of the University of Arizona Supersonic Wind Tunnel.

a Polaroid schlieren picture taken on the first run. Station barometric pressure readings were recorded hourly since the pressure transducer was referenced to atmospheric pressure. The recorder was calibrated by pumping down the vacuum tank to approximately 10 mm Hg absolute or less. The transducer was then connected to the tank vacuum line and simultaneous scale readings on the recorder and vacuum readings were taken for a series of points covering the range of the tests. Tank vacuum readings were taken with a McLeod vacuum gage.

A Polaroid schlieren picture was taken at the beginning of each series of runs. The Mach number and shock generator setting were then checked by direct measurement of angles from the schlieren photograph. Also, the shock wave interaction point and the separation point could be recorded for later analysis. For more detailed study, standard photographs were taken on high-speed fine-grain film.

For the series on laminar interactions, shock strengths were varied by adjusting the shock generator deflection angle from 4 degrees to 19 degrees in a number of steps. The Reynolds number of the interaction point varied slightly in the vicinity of 5.5×10^5. The Mach number was maintained at a constant $M = 3.2$ for all the tests.

Only two runs were made for the turbulent interaction. Shock strengths were set with deflection angles of 9 degrees and 15 degrees on the shock generator. The Reynolds number for turbulent interaction was in the vicinity of 7×10^5.

For the turbulent studies a .010 inch trip wire was affixed just downstream of the leading edge of the plate. To insure turbulent

interaction the shock generator was also moved rearward so that interaction took place approximately 4.0 to 4.5 inches from the leading edge.

3.3 Laminar Interactions

Theoretically, the separation pressure ratios and peak pressure can be predicted for any shock strength, Reynolds number, and Mach number below M = 4.0 using the approximation formulas developed in Chapter 2 and a set of shock tables. These values will be computed for each configuration tested and compared with the actual results. Finally, possible reasons for departure of the experimental results from the theoretical predictions will be advanced and recommended solutions proposed where applicable.

Table I is a tabulation of theoretical pressure rise for a regular shock wave reflection and actual experimental pressure rise for each shock strength investigated. Note that the experimental values are considerably lower than the theoretical values, especially for the higher shock strengths. This may be explained by the fact that the expansion wave from the trailing edge of the shock generator interacts with the boundary layer in the region of reattachment where the peak pressure should be. It is due in part to pressure "leak" from the upper surface to the lower surface of the plate. Problems with choking at high shock generator angles necessitated shortening the turning surface of the shock generator thereby moving the expansion wave closer to the interaction point. This problem could be solved by moving the shock generator closer to the plate or by

designing a shock generator that could be adjusted externally after the starting process. The latter solution would allow a longer shock generator surface which could be set at a low angle of attack for starting and then be adjusted to the desired angle after the starting process.

In computing the pressure ratio at separation, Equation (9) from Chapter 2 may be simplified since this study was accomplished at a constant Mach number M = 3.2. Therefore, Equation (9) becomes

$$\frac{P_s - P_1}{P_1} = \frac{0.78(1.4)(3.2)^2}{\left[(3.2^2-1)Re_{x_s}\right]^{1/4}} \left\{ \frac{\left[1+(.2)(3.2)^2\right]\left[1-\frac{0.636\tan^{-1}\left[(.2)^{1/2}(3.2)\right]}{\left[(.2)^{1/2}(3.2)\right]}\right]}{1+0.693(.4)(3.2)^2} \right\}$$

$$= \frac{6.42}{(Re_{x_s})^{1/4}}\left[.794(1-.427)\right]$$

$$\frac{P_s - P_1}{P_1} = \frac{2.92}{(Re_{x_s})^{1/4}}$$

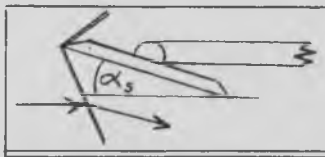	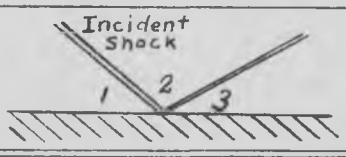	
Shock generator angle α_s	$\frac{p_3}{p_1}$ Regular reflection, theoretical	$\frac{p_3}{p_1}$ Boundary layer interaction, experimental
4°	1.82	2.000
8°	3.16	2.615
10°	4.40	2.840
15°	7.13	3.750
19°	10.80	4.680

Table I Theoretical and experimental total pressure rise ratios for various shock strengths, M = 3.2.

Shock Strength	Separation point, from leading edge	Re_{x_s}	p_s/p_1 Theoretical	p_s/p_1 Experimental
4°	1.93"	3.21×10^5	1.122	1.00
8°	2.23"	3.71×10^5	1.118	1.02
10°	2.16"	3.60×10^5	1.119	1.04
15°	2.50"	4.16×10^5	1.115	1.07
19°	1.75"	2.91×10^5	1.126	(1.125) approx.

Table II Theoretical and experimental parameters for pressure ratio at separation, laminar interaction, M = 3.2.

The above relationship shows that for a fixed Mach number, the separation pressure ratio is a function of Reynolds number only. Table II shows the various separation parameters for a given shock strength and a comparison of the theoretical vs. experimental values of separation pressure ratios. In Figure 3.05 is a graphical interpretation of these results. Note that the theoretical "hump" at the beginning of the curves has been incorporated for the 10^{o}, 15^{o} and 19^{o} cases. Although intermediate pressure readings were not available to confirm this configuration, the existing points lend themselves to predicting this phenomenon. Due to the fact that the plate was designed prior to the experience gained in this study, the pressure taps in this critical separation area are farther apart than would be desired to get an accurate pressure plot in this region.

Theoretically, the pressure should remain near its maximum value downstream of the reattachment point. However, Figure 3.05 shows a sharp drop in pressure downstream of the reattachment point and some unpredicted fluctuations. These phenomena are believed to be due to the reflected wave patterns seen in the schlieren photographs of Figure 3.06 and 3.07. It also appears that a second boundary layer is beginning to form and thicken downstream of the reattachment point where the reattached layer seems to dissipate. This phenomenon of a second boundary layer was not investigated further; however, it might prove interesting as another separate study.

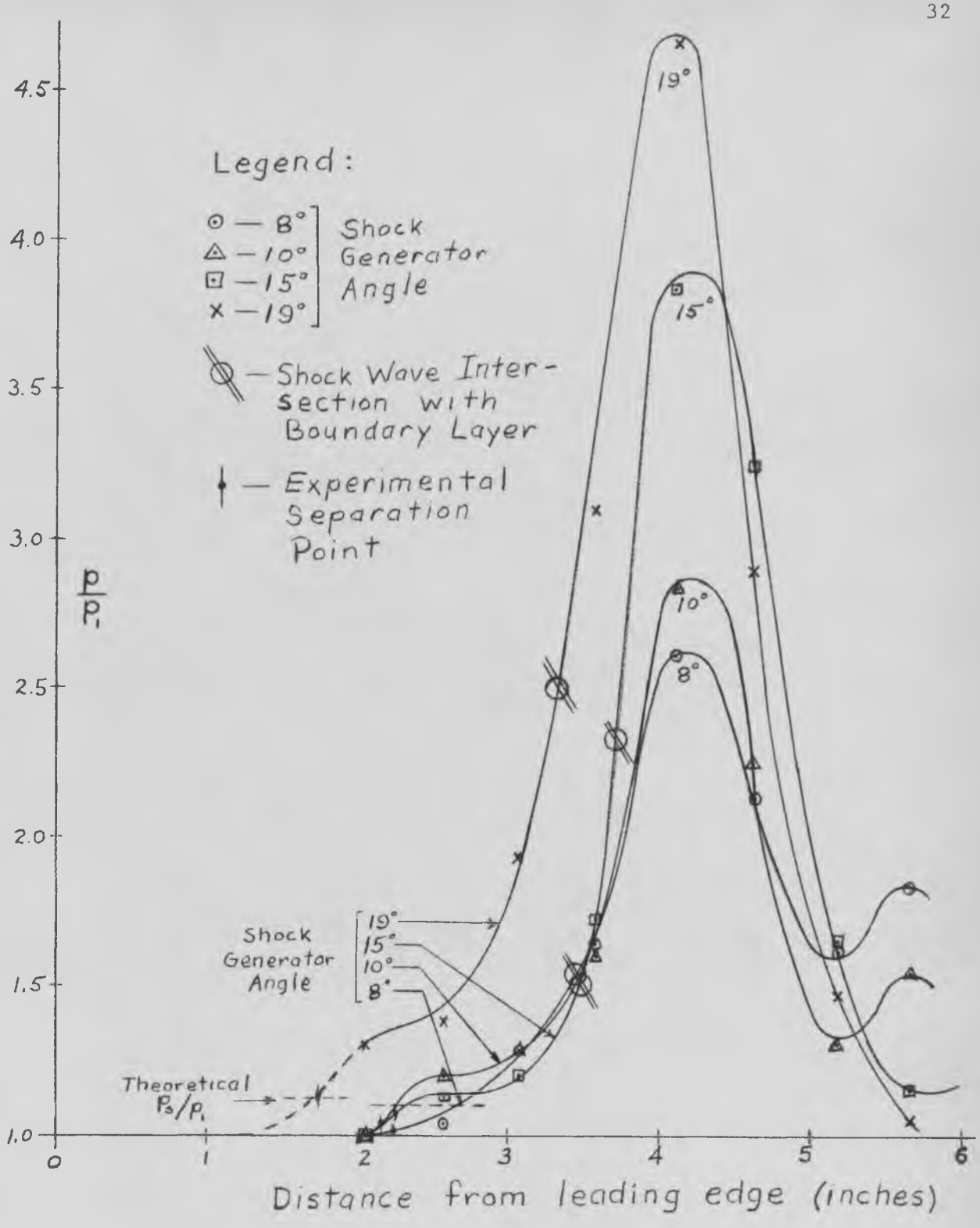

Figure 3.05 Experimental Curves for Shock Wave Interactions With a Laminar Boundary Layer.

Another phenomenon observed in the schlieren photographs is the thin shock-like wave preceding the main shock just upstream of the interaction point. A possible explanation is that this wave is the reflection from the side walls of the tunnel of the shock wave generated by the shock generator.

Mention should be made here that although the theory developed in Chapter 2 is assumed to apply to a wholly laminar flow, it is very possible that the boundary layer under consideration is in the transition region at the point of impingement of the shock wave. The lower limit for the point of transition is regarded by Schlicting (Ref. 7) to be $Re_{x_{crit}} = 3.2 \times 10^5$, varying up to $Re_{x_{crit}} = 10^6$ and higher for exceptionally disturbance-free external flow. The points of impingement in this study ranged from $Re_x = 5.5 \times 10^5$ to $Re_x = 5.8 \times 10^5$ for the assumed laminar cases.

A few modifications which might improve some of the above situations are as follows:

(1) Construct pressure taps farther forward and closer together longitudinally on the plate. This would provide for a lower Reynolds number at the shock interaction point and also allow a more accurate pressure traverse in the critical regions.

(2) Redesign the test model to span the whole test section, being supported at the sides rather than at the center. A cleaner configuration may be possible to reduce the interacting reflections on the plate as well as avoiding the three-dimensional effects from

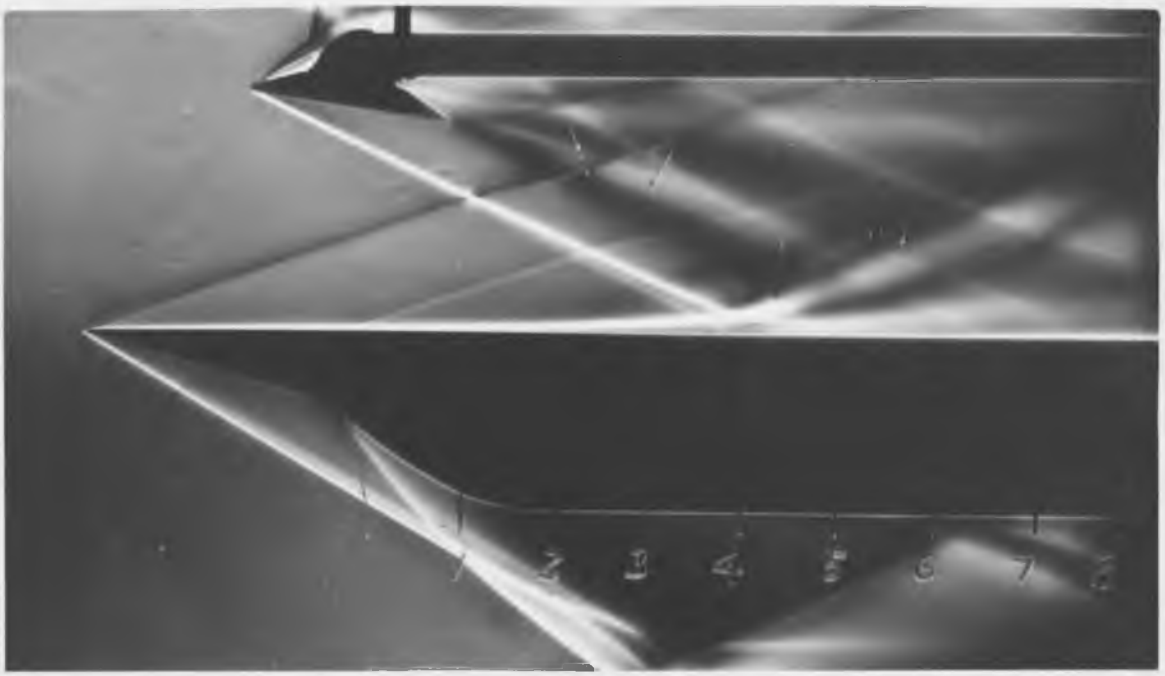

(a)

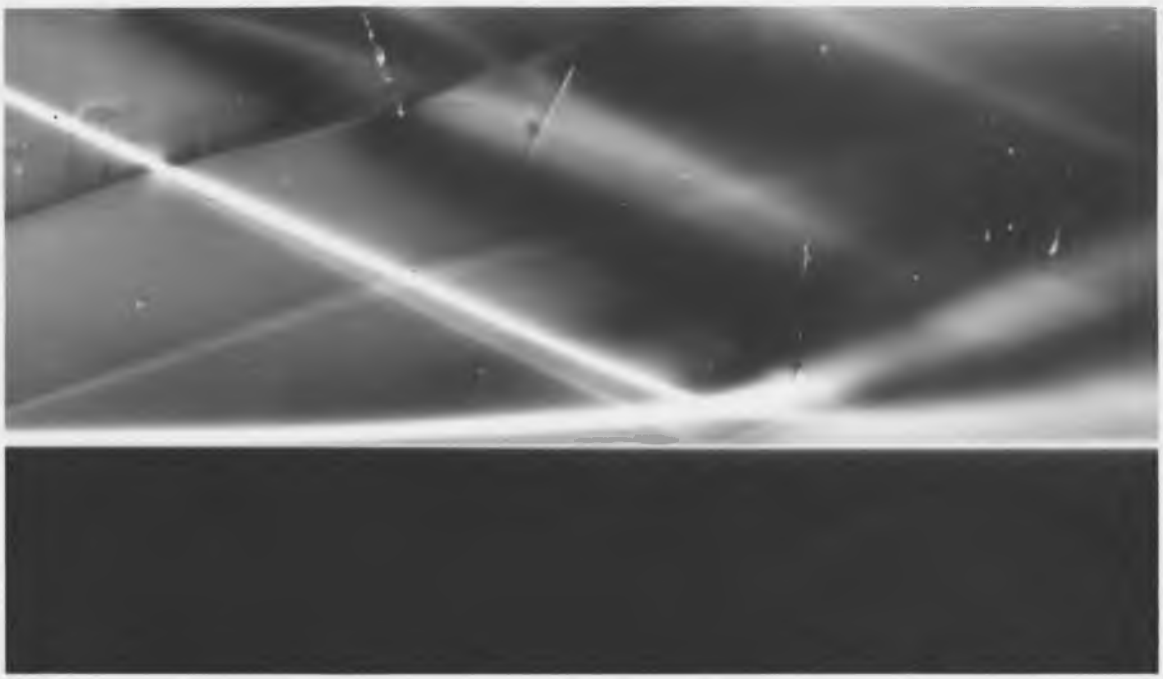

(b)

Figure 3.06 Schlieren photographs of laminar interaction with shock generator angle at 8^{o}. (a) View of test model; (b) enlarged interaction area.

(a)

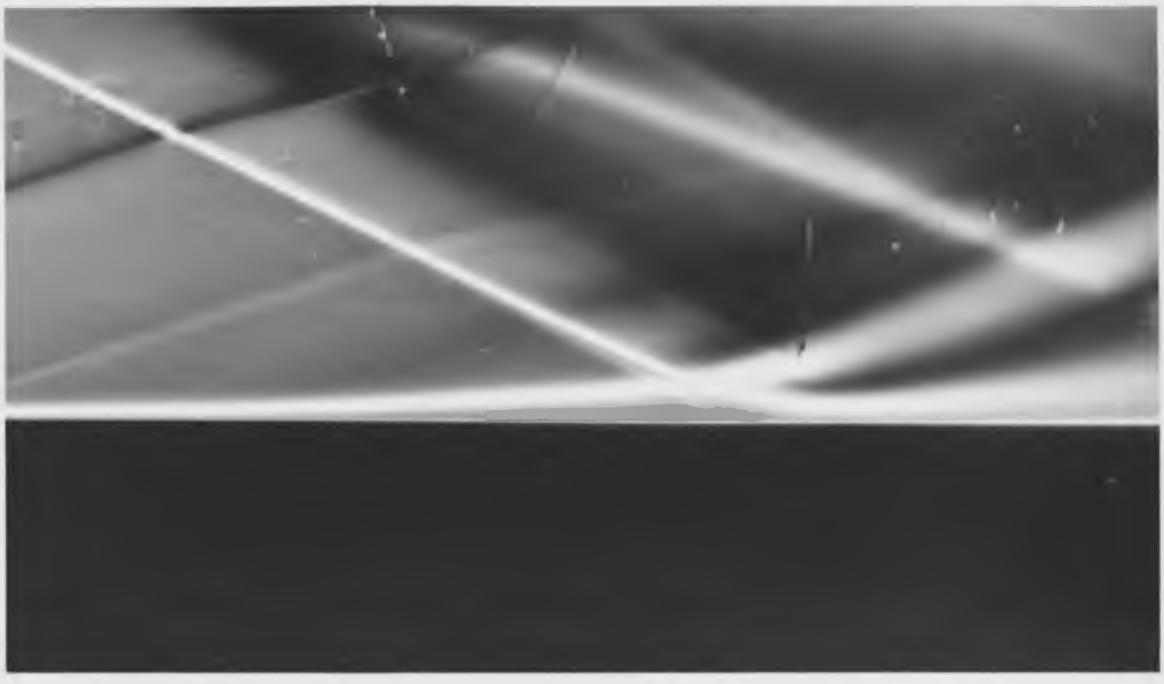

(b)

Figure 3.07 Schlieren photographs of laminar interaction with shock generator angle at 10^{o}. (a) View of test model; (b) enlarged interaction area.

the side walls and would tend to reduce pressure "leak" from the upper surface to the lower surface of the plate. An external adjustment capability for the shock generator, mentioned previously, might also be incorporated.

The laminar boundary layer-shock wave interaction phenomena as measured by experiment corresponded fairly well to predicted theoretical values. The argument that the separation point depends upon freestream Mach number and Reynolds number alone seems to be valid. It is also reasonable to believe that the total pressure rise through the interaction would approach the theoretical regular reflection pressure rise in the absence of the above mentioned problems. Generally, the results of experiment correlated rather well with theoretical predictions.

3.4 Turbulent Interactions

As previously mentioned, for the turbulent studies a .010 inch trip wire was affixed just downstream of the leading edge of the plate to hasten transition to turbulent flow. The shock interaction point was moved downstream also to obtain a Reynolds number in the vicinity of $Re_x = 7 \times 10^5$ which would insure turbulent interaction. Runs were made at two shock strengths, 9 degree- and 15 degree-shock generator angles. These strengths were chosen to compare the effects of a shock just strong enough to initiate separation with a strong shock which caused greater separation. The validity of Equation (10) will be checked in this section and the effects of turbulent interaction will be compared graphically with the laminar case of Section 3.3.

Table III compares the theoretical and experimental separation parameters as was done for the laminar case. Figure 3.08 shows the curves as determined experimentally with the observed and predicted separation points indicated. The laminar interaction curve for a 15° shock strength is compared with the turbulent interaction of the same shock strength in Figure 3.09. The curves are superimposed at the shock interaction point to show the comparison more clearly with the Reynolds number of the point of impingement shown for each case.

Shock Generator Angle α_s	9°	15°
$\frac{P_s}{P_1}$ Theoretical	2.64	2.64
Approx. P_s/P_1 Experimental	2.03	2.22
Shock Interaction Re_x	7.55×10^5	7.48×10^5

Table III Comparison of theoretical predictions and experimental results for turbulent interaction.

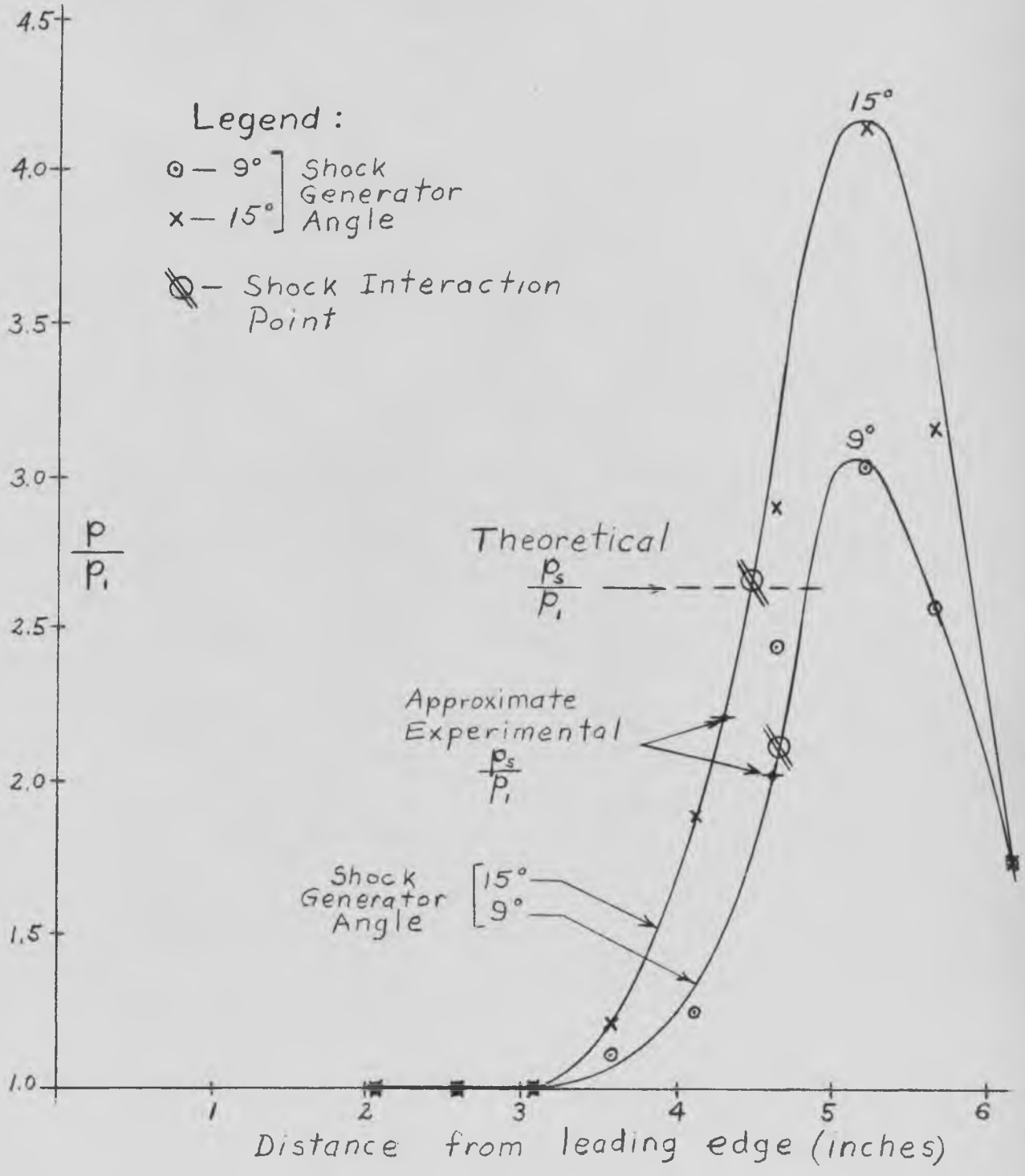

Figure 3.08 Experimental Curves for Shock Wave Interaction With a Turbulent Boundary Layer.

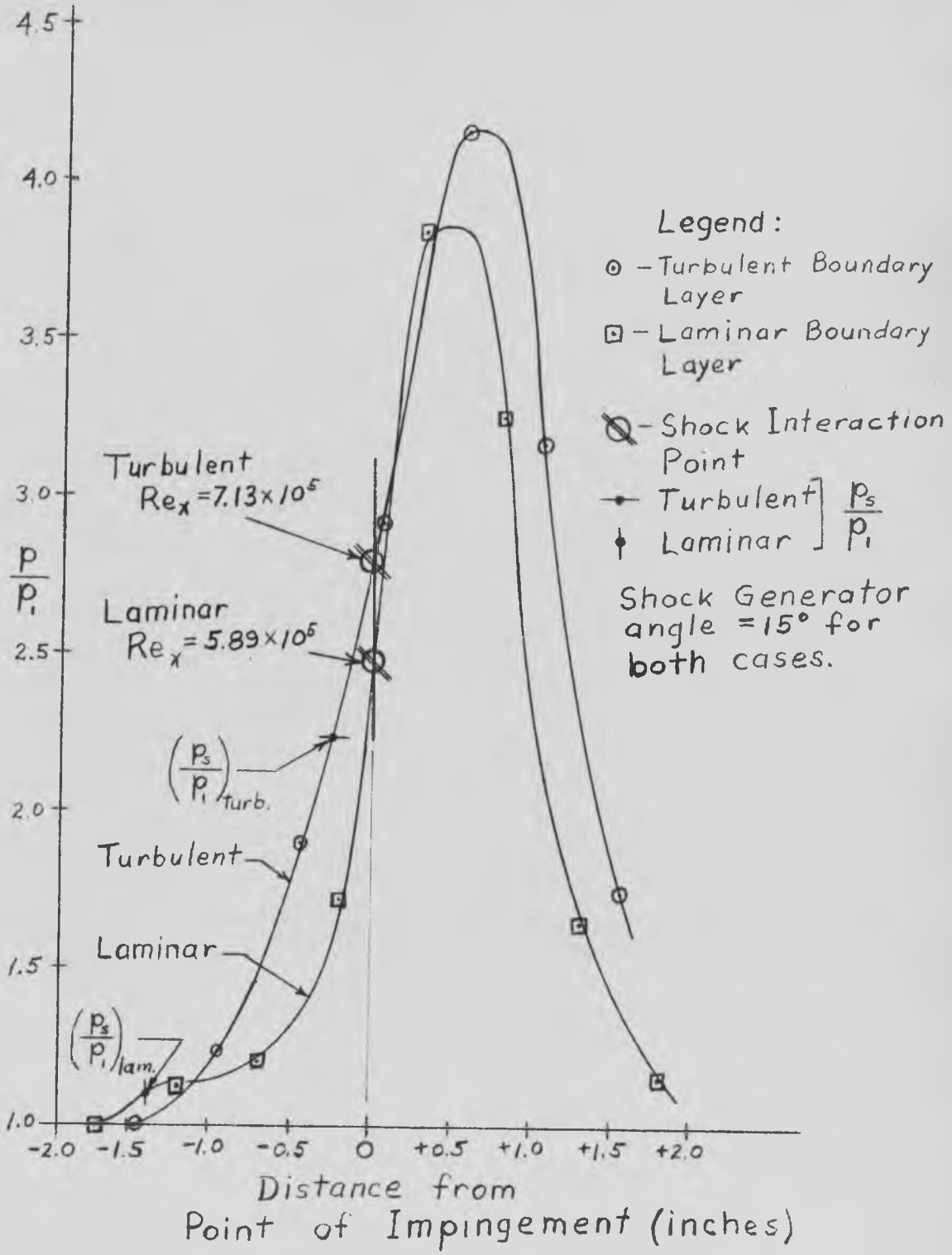

Figure 3.09 Comparison of Experimental Curves for Laminar and Turbulent Interactions With Shock Strengths Approximately Equal.

For the study under consideration, Equation (10) becomes

$$\frac{p_s}{p_1} = \left[\frac{1+.2\,(3.2)^2}{1+0.64(.2)(3.2)^2}\right]^{\frac{1.4}{4}} = \left[\frac{1+2.05}{1+1.31}\right]^{3.5}$$

$$\therefore \frac{p_s}{p_1} = 2.64$$

This value was found to be higher than the experimental values measured from the schlieren photographs. Experiments by Kepler and Bogdonoff (Ref. 3) gave results similar to those obtained in this study, that is $\frac{p_s}{p_1}$ values just above $\frac{p_s}{p_1} = 2.0$. No firm reason can be given for this difference, but differences in model configuration seems to affect the results dependent upon the degrees of two-dimensional flow obtained. Gadd (Ref. 1) mentioned this fact in his presentation before the Boundary Layer Research Symposium (Ref. 8) at Freiburg, Germany, in 1957. However, most recent experimental work tends to agree on a value of $\frac{p_s}{p_1}$ in the range of 2.0 to 2.2 for a Mach number of 3.2.

Comparison of the turbulent layer interaction with that of the laminar case confirms in general the theoretical reasoning of Chapter 2. The pressure does not propagate quite as far forward of the interaction point in the turbulent layer, probably due to the reduced thickness of the subsonic boundary layer. Also notable is the fact that the turbulent layer takes a much higher pressure gradient to cause separation, almost by a factor of two. As explained in Chapter 2, the turbulent boundary layer is able to withstand an adverse pressure gradient better than a laminar boundary layer due to mass acceleration effects and

the greater momentum of the layer due to turbulence. This explains the physical phenomena seen in the schlieren photographs of Figures 3.10 and 3.11 where boundary layer separation is much closer to the shock interaction point than in the laminar case.

Noticeable by its absence in the turbulent case is the "hump" in the pressure curve of the laminar interaction. The turbulent pressure curve rises steeply from the beginning with not much hint of a leveling-off point until the peak pressure is reached. The peak pressure is still far below the theoretical maximum calculated for a regular reflection, although the turbulent peak was higher than for the laminar case. The explanation seems to be due to the pressure "leak" mentioned previously and to the effects of the expansion wave interaction from the trailing edge of the shock generator. The higher peak pressure for the turbulent interaction suggests that the turbulent boundary layer is much less susceptible to external disturbances than the laminar boundary layer, and in general this seems to hold true.

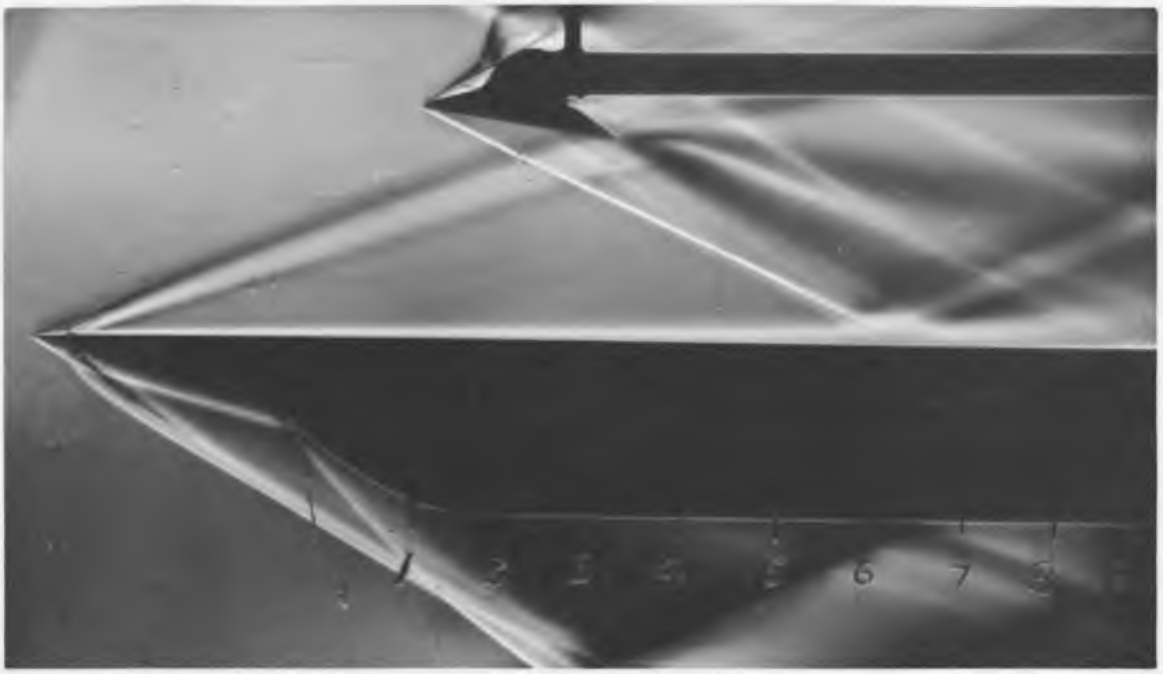

(a)

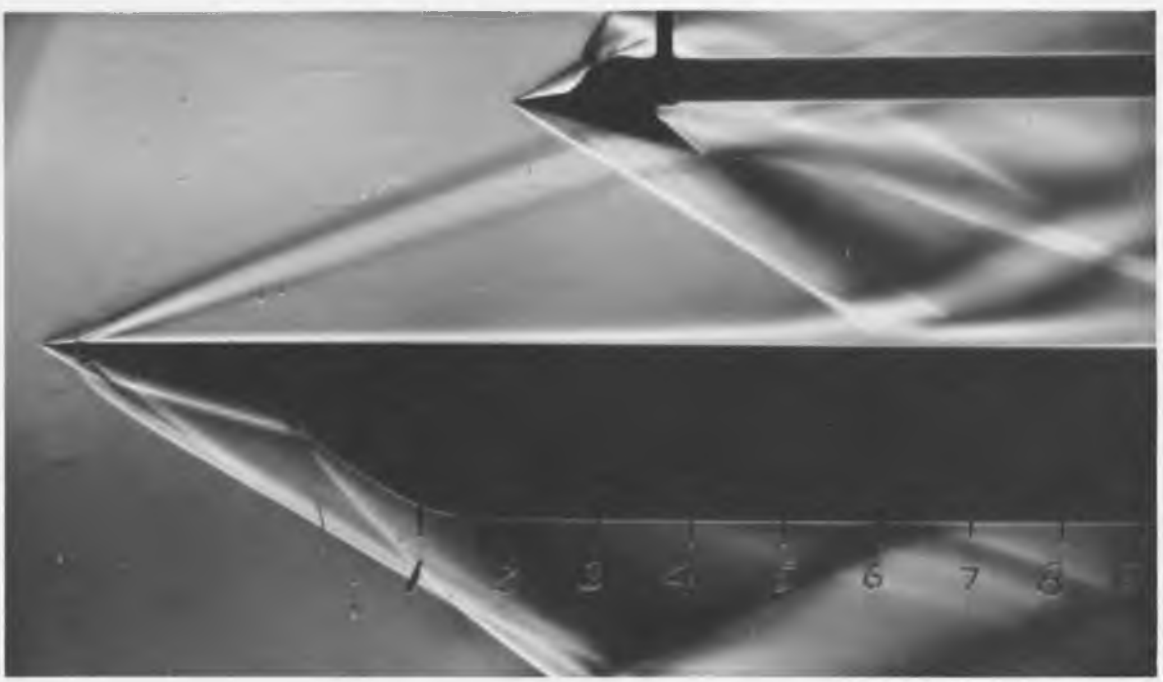

(b)

Figure 3.10 Schlieren photographs of turbulent interaction. (a) Shock generator angle at 9^{o}; (b) shock generator angle at 15^{o}.

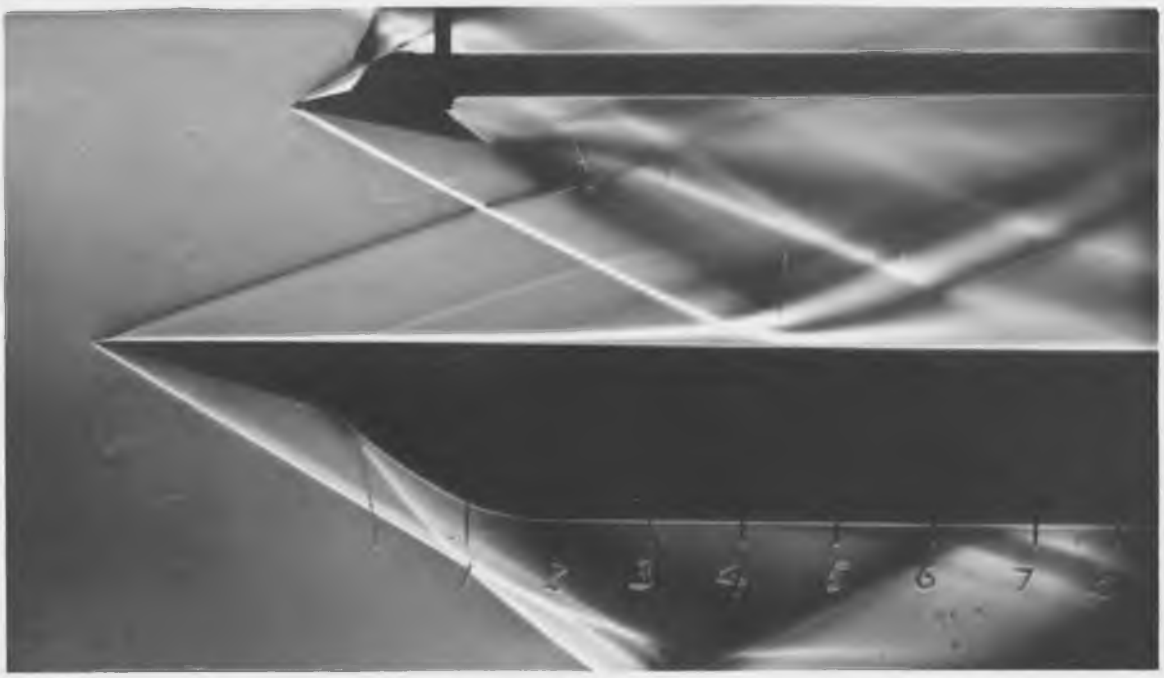

(a)

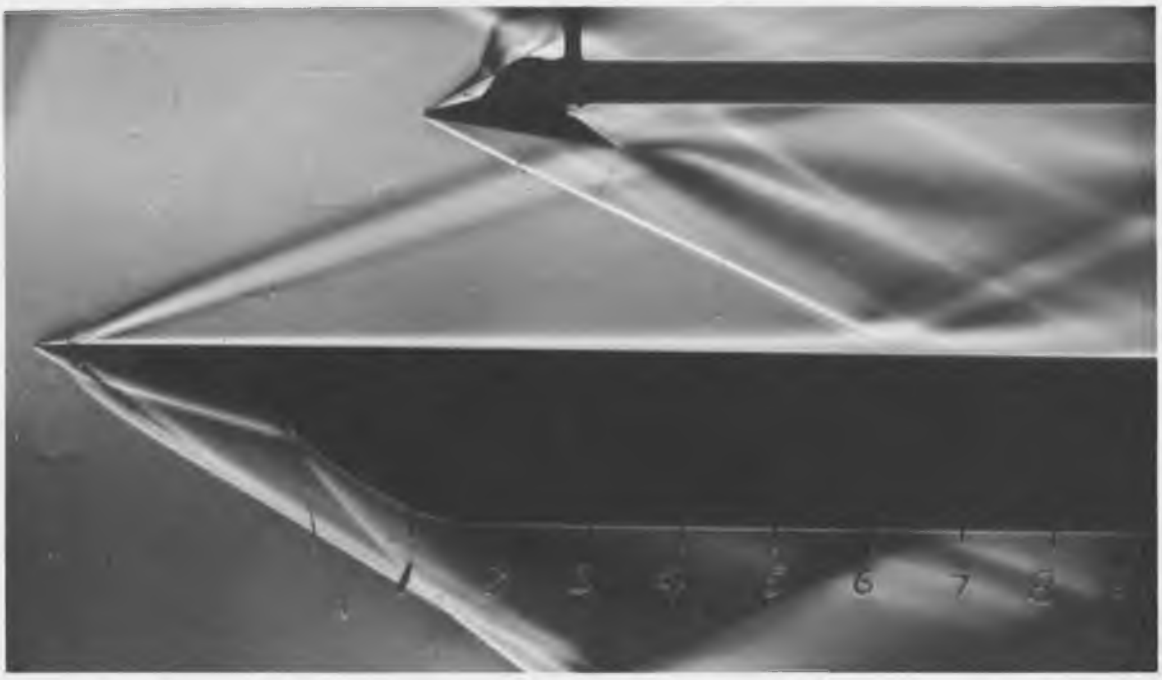

(b)

Figure 3.11 Comparison of laminar and turbulent interaction. (a) Laminar interaction with shock generator angle at 10^{o}, (b) turbulent interaction with shock generator angle at 9^{o}.

3.5 Conclusions

From the experimental investigation it may be concluded that pressures are indeed propagated within a boundary layer, both upstream and downstream of the point of impingement of an external shock wave. Pressure gradients are introduced which may cause the boundary layer to separate depending upon the shock strength, Reynolds number, and freestream Mach number. For laminar boundary layers the pressure ratios for separation are much smaller in general than for turbulent boundary layers and are a function of Reynolds number and Mach number. Peak pressures downstream of the interaction were found to be much lower than for the theoretical regular reflection, but this was due in part to the interaction of the expansion wave from the rear of the shock generator. With a redesigned shock generator configuration and with a model spanning the entire width of the test section this problem can be reduced and results should show an overall pressure rise just slightly lower than the theoretical value. This result has been obtained by other researchers investigating shock wave-boundary layer interaction. Laminar investigation also revealed that the boundary layer separated even for very low shock strengths. This should be expected since separation pressure ratios, predicted and observed, were very low and the weakest shock investigated caused a pressure rise much greater than critical. It may be concluded that laminar boundary layers, although very similar to turbulent layers in the interaction configuration, are very sensitive to external disturbances and separate quite readily.

Pressure ratios for separation of turbulent boundary layers were found experimentally to be much higher than for laminar cases, although not quite as high as predicted theoretically. The critical pressure ratio seems to be fairly constant for both shock strengths investigated. The turbulent layers required a much stronger shock to make them separate. It may be concluded that turbulent boundary layers are much less sensitive to external disturbances than laminar layers and tend to resist longitudinal pressure gradients for fairly strong shock strengths.

3.6 Areas of Interest Requiring Further Investigation

Several recommendations for further consideration and investigation are as follows:

(1) More accurate investigation of the critical initial separation area in both laminar and turbulent boundary layers;

(2) Investigation of the build-up of a "second" boundary layer observed in the schlieren photographs after the apparent dissipitation of the original boundary layer downstream of the reattachment point;

(3) Redesign of the test model for minimum extraneous disturbances such as reflected shock waves and expansion waves, and elimination of three-dimensional effects.

(4) Further theoretical analysis for turbulent boundary layer prediction of separation;

(5) Spark schlieren photographs of interaction phenomena permitting an exposure in the vicinity of one microsecond. This would

allow a more detailed examination of the instantaneous conditions of the boundary layer, particularly for the turbulent studies.

REFERENCES AND SELECTED BIBLIOGRAPHY

1. Gadd, G. E. "Interactions Between Wholly Laminar or Wholly Turbulent Boundary Layers and Shock Waves Strong Enough to Cause Separation," Journal of Aeronautical Sciences, Vol. 20, p. 729 (1953).

2. Barry, F. W., Shapiro, A. H., and Neumann, E. P. "The Interaction of Shock Waves With Boundary Layers on a Flat Surface," Journal of Aeronautical Sciences, Vol. 18, p. 229 (1951).

3. Kepler, C. E., and Bogdonoff, S. M. "Study of Shock Wave-Turbulent Boundary Layer Interaction at M = 3." Princeton University Aeronautical Engineering Department. Report 222, July, 1953.

4. Young, A. D. "Skin Friction in Compressible Flow," The Aeronautical Quarterly, Vol. 1, 1949.

5. Liepmann, H. W., and Roshko, A. Elements of Gasdynamics. New York: John Wiley and Sons, Inc., 1957.

6. Monaghan, R. J., and Johnson, J. R. "Boundary Layer Measurements on a Flat Plate at M = 2.5 and Zero Heat Transfer," British A.R.C., C.P. 64, 1949.

7. Schlicting, H. Boundary Layer Theory. 4th ed. New York: McGraw-Hill Book Co., Inc., 1962.

8. Gadd, G. E. "Interaction Between Shock Waves and Boundary Layers," Symposium on Boundary Layer Research, Freiburg, Germany, August 1957, H. Goertler, ed., Springer-Verlag, Berlin, 1958.

9. Bogdonoff, S. M., and Kepler, C. E. "Separation of a Supersonic Turbulent Boundary Layer," Journal of Aeronautical Sciences. Vol. 22, p. 414 (1955).

10. Chapman, D. R., Kuehn, D. M., and Larson, H. K. "Investigation of Separated Flows in Supersonic and Subsonic Streams," NACA TN 3869, Washington, D.C., March 1957.

11. Fage, A., and Sargent, R. "Shock Wave and Boundary Layer Phenomena Near a Flat Plate Surface," Proceedings of the Royal Society, A 190, p. 1 (1947).

12. Gadd, G. E., Holder, D. W., and Regan, J. D. "An Experimental Investigation of the Interaction Between Shock Waves and Boundary Layers," Proceedings of the Royal Society, A226, p. 227 (1954).

13. Honda, M. "A Theoretical Investigation of the Interaction Between Shock Waves and Boundary Layers," Journal of Aeronautical and Space Sciences, Vol. 25, p. 667 (1958).

14. Mager, A. "Prediction of Shock - Induced Turbulent Boundary-Layer Separation," Journal of Aeronautical Sciences, Vol. 22, p. 201 (1955).

15. Pearcy, H. H. "Shock Induced Separation and Its Prevention," Boundary Layer and Flow Control, G. V. Lachmann, ed., London: Pergamon Press, 1961.

16. Schuh, H. "On Determining Turbulent Boundary Layer Separation in Incompressible and Compressible Flow," Journal of Aeronautical Sciences, Vol. 22, p. 343 (1955).

17. Shapiro, A. H. The Dynamics and Thermodynamics of Compressible Fluid Flow, Vol. 2. New York: The Ronald Press Co. 1954.

18. Tyler, R. D., and Shapiro, A. H. "Pressure Rise Required for Separation in Interaction Between Turbulent Boundary Layer and Shock Wave," Journal of Aeronautical Sciences, Vol. 20, p. 858 (1953).